Article

Neuron

Characterising Microglia in *App* Knock-in Mouse Models of Alzheimer's Disease

Highlights

- Genes associated with microglial phagocytic activity are substantially upregulated in the cortex of 9-month *App*$^{NL\text{-}G\text{-}F/NL\text{-}G\text{-}F}$ mice, compared to wildtype controls.
- Microglial proliferation and antigen presentation increase in the hippocampus of 9-month *App*$^{NL\text{-}G\text{-}F/NL\text{-}G\text{-}F}$ mice. 9-month *App*$^{NL\text{-}F/NL\text{-}F}$ and 4-month *App*$^{NL\text{-}G\text{-}F/NL\text{-}G\text{-}F}$ mice do not show these changes.
- Polarisation of microglia to pro- and anti-inflammatory states are not significantly different in 9-month *App*$^{NL\text{-}G\text{-}F/NL\text{-}G\text{-}F}$ mice compared to wildtype controls.

CellPress

Neuron

Article

Characterising Microglia in *App* Knock-in Mouse Models of Alzheimer's Disease

Victoria Smith [1]

[1]Department of Neuroscience, Physiology and Pharmacology, University College London, Gower St, London, UK

SUMMARY

Transgenic models of Alzheimer's disease (AD) overexpressing amyloid precursor protein (APP) have been criticised for generating artefactual results and held accountable for limited success in translating results from mouse studies to human AD clinical trials. The recent publications of *App* knock-in (*App*-KI) models, containing combinations of human familial Swedish (NL), Arctic (G) and Beyreuther-Iberian (F) mutations, offer improved models. Although microglia are emerging as a key player in human AD from both GWAS and animal studies, the microglial phenotype of these *App*-KIs is not well understood. Consequently, this research aims to assess microglial numbers, activation status and gene expression in the App-KI models, to understand how their phenotype reflects human disease progression. Tissue from homozygous $App^{NL\text{-}F/NL\text{-}F}$ or $App^{NL\text{-}G\text{-}F/NL\text{-}G\text{-}F}$ mice of age 4- and 9-months were used to compare microglial differences at different stages of amyloid-beta pathology. Immunohistochemical procedures were used to quantify microglial numbers in the hippocampus. Results show microglial proliferation in $App^{NL\text{-}G\text{-}F/NL\text{-}G\text{-}F}$ mice at 9-months. Quantitative PCR in $App^{NL\text{-}G\text{-}F/NL\text{-}G\text{-}F}$ cortex at 9-months indicates large increases in expression of several microglial genes, associated with phagocytic activity, such as *Trem2* and *Cd68*, but no changes in microglial inflammatory polarity. Collectively, these results suggest microglia are responding to amyloid pathology by increasing their phagocytic activity, most probably against dystrophic neurites and Aβ plaques.

INTRODUCTION

Alzheimer's Disease (AD), characterised by a long prodromal phase of around 20 years where pathology is present before symptoms manifest, is the leading cause of Dementia. AD pathology consists of two major hallmarks: amyloid-beta (Aβ) plaques and neurofibrillary tangles. AD pathology spreads throughout the brain as the disease progresses. Aβ plaques form extracellularly from accumulation of insoluble Aβ-peptides. Aβ-peptides are formed from cleavage of amyloid precursor protein (APP) by β- and γ-secretase enzymes (Haass et al., 2012). Neurofibrillary tangles are formed by aggregation of abnormally hyperphosphorylated microtubule associated protein tau. AD is also associated with increases in microglial and astrocyte numbers and activity, and neuroinflammation, including increased inflammatory cytokines. These pathologies cumulatively contribute to synaptic dysfunction and neuronal death, resulting in progressive cognitive decline.

In the healthy adult brain, microglial cells are involved in maintaining brain homeostasis, by detecting and phagocytosing pathogens and debris (Nimmerjahn et al., 2005). Microglia, typically found in a surveillance state (Hanisch and Kettenmann, 2007), scan the local area for homeostatic changes, such as infectious agents and damaged neurons by rapidly extending and retracing their processes, making temporary contacts with surrounding neurons, glia and blood vessels (Davalos et al., 2005; Nimmerjahn et al., 2005). In response to brain trauma or pathology, microglial morphology and gene expression is altered, and they migrate to the site of damage, to phagocytose cell debris and pathogens. Depending on activation cues, microglia can take on distinct phenotypes. In general terms, microglia can be polarised towards a pro- or anti-inflammatory phenotype. Pro-inflammatory microglia are associated with producing inflammatory cytokines, and reactive oxygen species, whereas anti-inflammatory microglia produce anti-inflammatory cytokines, and carry out wound repair and debris clearance (Cherry et al., 2014). Anti-inflammatory microglia are typically associated with more efficient Aβ phagocytosis whereas the pro-inflammatory phenotype may inhibit this (Koenigsknecht-Talboo and Landreth, 2005; Michelucci et al., 2009). However, it is becoming increasingly likely that microglial activation states represent more of a continuum (Mosser and Edwards, 2008). A spectrum of phenotypes can be expressed in the brain simultaneously, as seen in human brain injury (Morganti et al., 2016). The balance of the pro- and anti-inflammatory phenotypes present may determine microglial responses to stimuli. In AD, this careful balance could be lost, reducing effective, appropriate microglial function and leading to loss of brain homeostasis.

Microglia are more prolific in AD brains and switch from a predominantly anti-inflammatory to pro-inflammatory phenotype in the brain across AD, in post-mortem tissue (Hoozemans et al., 2006; Jimenez et al., 2008). These changes could contribute to the loss of brain homeostasis in AD. A number of microglial risk genes for AD such as *TREM2, ABI3* and *PLCG2*, have emerged from Genome Wide Association studies (GWAS) (Guerreiro et al., 2013; Lambert et al., 2013; Sims et al., 2017) in recent years, demonstrating the critical involvement of microglia in AD. Moreover, microglial phenotype has been shown to change with age, including expressing genes which confer susceptibility to AD (Olah et al., 2018) explaining, to some extent, why age is a risk factor in AD. Tracers for microglial activation and Aβ deposition have allowed the *in vivo* relationship of these factors to be assessed, in AD patients. Microglial activation was positively correlated with fibrillar Aβ deposition, in both prodromal and severe AD (Hamelin et al., 2016), supporting a change in microglia with Aβ pathology. Further understanding of these microglial phenotypes, and how they change across AD, is needed.

Transgenic models overexpressing human *APP* have been criticised, as overexpression of *APP* can lead to excessive production of active APP fragments, other than Aβ, which is not representative of human AD, producing artefacts. To tackle these criticisms, *App* knock-in (*App*-KI) models have been recently generated as improved models in which to study AD (Saito et al., 2014). The Aβ region of the *App* gene in mice was humanised and human familial autosomal dominant mutations were inserted here. *App*-KI mice avoid disadvantages of transgenic models, by maintaining the endogenous murine locus, ensuring normal expression levels of the *App* products in the relevant specific cells types. *App*-KI mice show an increase in Aβ pathology, synapse loss, astrocyte activation and microglial numbers in an age-dependent manner. The age and aggressiveness of Aβ deposition has been well characterised in these models (Saito et al., 2014) but microglial changes have not.

I focus on the $App^{NL\text{-}F/NL\text{-}F}$ and $App^{NL\text{-}G\text{-}F/NL\text{-}G\text{-}F}$ strains of *App*-KI mice. $App^{NL\text{-}F/NL\text{-}F}$-KI mice have two mutations, inserted into the mouse *App* gene. Firstly, KM670/671NL (Swedish), just upstream of the amino acid sequence of Aβ, increases the total amount of $Aβ_{1\text{-}40}$ and $Aβ_{1\text{-}42}$, by increasing the cleavage of APP by β-secretase (Citron et al., 1992). Secondly, 1716F (Iberian/Beyreuther), just downstream of the coding region of $Aβ_{1\text{-}42}$, increases the ratio of $Aβ_{1\text{-}42}$ to $Aβ_{1\text{-}40}$, by increasing the cleavage by γ-secretase at the $Aβ_{1\text{-}42}$ cleavage site (Guardia-Laguarta et al., 2010). $App^{NL\text{-}F/NL\text{-}F}$ mice have the human wildtype Aβ sequence, resembling human sporadic AD, but elevated Aβ and an increased ratio of $Aβ_{1\text{-}42}$ to $Aβ_{1\text{-}40}$, making the Aβ more likely to aggregate. $Aβ_{1\text{-}42}$ increases in an age dependent manner giving a progressive Aβ pathology with initial Aβ deposition at 6 months (Saito et al., 2014). $App^{NL\text{-}G\text{-}F/NL\text{-}G\text{-}F}$ mice have an additional mutation, E693G (Artic), in the coding region for Aβ, altering the $Aβ_{1\text{-}42}$

amino acid sequence. This causes a conformational change in $A\beta_{1-42}$ making it more prone to aggregate (Tsubuki et al., 2003), producing a more aggressive phenotype with Aβ being deposited and plaques forming at younger age, around 3-4 months (Saito et al., 2014), and being quite prolific by 9-months. Notably, these mice represent early stages of AD pathology, and never display neurofibrillary tangles or neuronal death. This is a limitation for drug development, as drugs which have efficacy in these mice will likely only have efficacy in early preclinical AD. However, therapeutic intervention at early disease stages is becoming more realistic, with increasingly sophisticated diagnostic tools. Thus, understanding how microglia behave in these sophisticated mouse models may provide opportunities for drug discovery in early preclinical AD, to allow targeting of microglia specifically.

This study aimed to characterise microglia numbers and activation states in the different *App*-KI models. I hypothesised that proliferation and activation of microglia would increase with progressing amyloid pathology, and that *Trem2* will be upregulated by several-fold, as has been observed previously in *APP-PSEN1* mice in our lab (Liu, 2017). Hence, I would predict the $App^{NL\text{-}F/NL\text{-}F}$ mice to show these microglial changes from 9-months, and $App^{NL\text{-}G\text{-}F/NL\text{-}G\text{-}F}$ mice to show these changes from 4-months when they both begin to show Aβ plaques. Here, I report microglial proliferation in the hippocampus at 9-months $App^{NL\text{-}G\text{-}F/NL\text{-}G\text{-}F}$ mice and a substantial increase in expression of several microglial genes, associated with phagocytic activity, but no changes in microglial polarity in the cortex. Together, results suggest microglia are acting to phagocytose dystrophic neurites or Aβ plaques in these models, once amyloid pathology is well established.

RESULTS

Microglial proliferation and activity changes with progression of Amyloid Pathology in the hippocampus of *App*-KI mice

As the $App^{NL\text{-}G\text{-}F/NL\text{-}G\text{-}F}$ mice get plaques at around 4-months, whereas in the $App^{NL\text{-}F/NL\text{-}F}$ mice plaques are not detectable until 9-months, I have investigated these two time points in the different strains respectively, to compare them at approximately the same stages of amyloid pathology. To investigate microglial proliferation and activation with amyloid pathology development, immunohistochemistry was carried out in the hippocampus of *App*-KI mice. CA1 was selected, as this receives input both directly and indirectly from the Entorhinal cortex, and these pathways are severely affected by AD (Anand and Dhikav, 2012). Hemispheres of brains fixed by immersion in 4% paraformaldehyde, were immune-stained with antibodies against allograft ionised calcium binding adaptor molecule 1 (IBA1) and Cluster of

Differentiation 68 (CD68), from the brains of 4-month and 9-month *App*-KI mice, representing the initial and more developed stages of amyloid pathology, and in age matched wildtype (WT) controls. In the healthy brain, IBA1 is specifically expressed by microglia (Imai et al., 1996; Ito et al., 1998) in both surveillance and activation states and so can be used to represent the total microglial population. CD68, a lysosomal glycoprotein, expressed by microglia (Walker and Lue, 2015), is a marker of phagocytic activity. Total microglia in 3 sub-regions, the stratum pyramidum (SP), the stratum radiatum (SR) and the stratum lacunosum moleculare (SLM), of CA1 were quantified from images taken on the EVOS® FL Auto-Cell Imaging System (Figure 1A). Overall, microglial density, represented by IBA1+ cell density, shows a highly significant interaction between age and genotype, within each sub-region of the CA1, ($p<0.0001$, Generalised linear mixed model (GLMM), n=5 animals per group). Consistent with increase in amyloid pathology progression, $App^{NL\text{-}G\text{-}F/NL\text{-}G\text{-}F}$ mice had a greater density of microglia at 9-months compared to WT controls and 4-months $App^{NL\text{-}G\text{-}F/NL\text{-}G\text{-}F}$ mice in the SR ($p<0.01$ and $p<0.0001$ respectively, sequential Sidak test, n=5 animals) and SLM ($p<0.0001$) of CA1 (Figure 1D). Interestingly, 4-month $App^{NL\text{-}G\text{-}F/NL\text{-}G\text{-}F}$ mice did not show significant differences in microglial density compared to WT controls in any region, despite having numerous Aβ plaques at this point. Also, surprisingly, 9-month $App^{NL\text{-}F/NL\text{-}F}$ mice, in which sparse Aβ plaques are observed, show a similar trend, for increased microglial density in the SR ($p=0.082$) and SLM ($p=0.055$), to $App^{NL\text{-}G\text{-}F/NL\text{-}G\text{-}F}$ mice, in which amyloid pathology is much more well developed. No significant differences in microglial density was seen between any group in the SP between ages or genotypes. The proportion of IBA1+ cells which were CD68+, were also quantified in the same regions of CA1. This proportion was taken rather than quantifying CD68 alone, to see any changes in the number of cells expressing CD68 that is not just due to increase in total numbers of microglia. Almost all microglia (IBA1-positive cells) showed some CD68 immuno-fluorescence, so only cells which had CD68 expression (fluorescence) over the threshold (Figure 1B) were counted. A highly significant interaction between age and genotype was seen for CD68+/ IBA1+ cells, within each sub-region of CA1 ($p<0.0001$, GLMM, n=5 animals per group) but there were no statistically significant results from the post-hoc test. However, a similar trend can be observed in the SLM, to the trend seen with IBA1-positive cell density alone, where 9-month $App^{NL\text{-}G\text{-}F/NL\text{-}G\text{-}F}$ and $App^{NL\text{-}F/NL\text{-}F}$ mice show a tendency for similar increases in activation compared to 4-month $App^{NL\text{-}G\text{-}F/NL\text{-}G\text{-}F}$ mice and WT controls. This is not significant, likely due to variation between mice (Figure 1E). Overall, these results suggest that microglia in the 9-month $App^{NL\text{-}G\text{-}F/NL\text{-}G\text{-}F}$ mice proliferate in response to the well-developed amyloid plaques at this age, but not at 4-months of age when plaques first start developing.

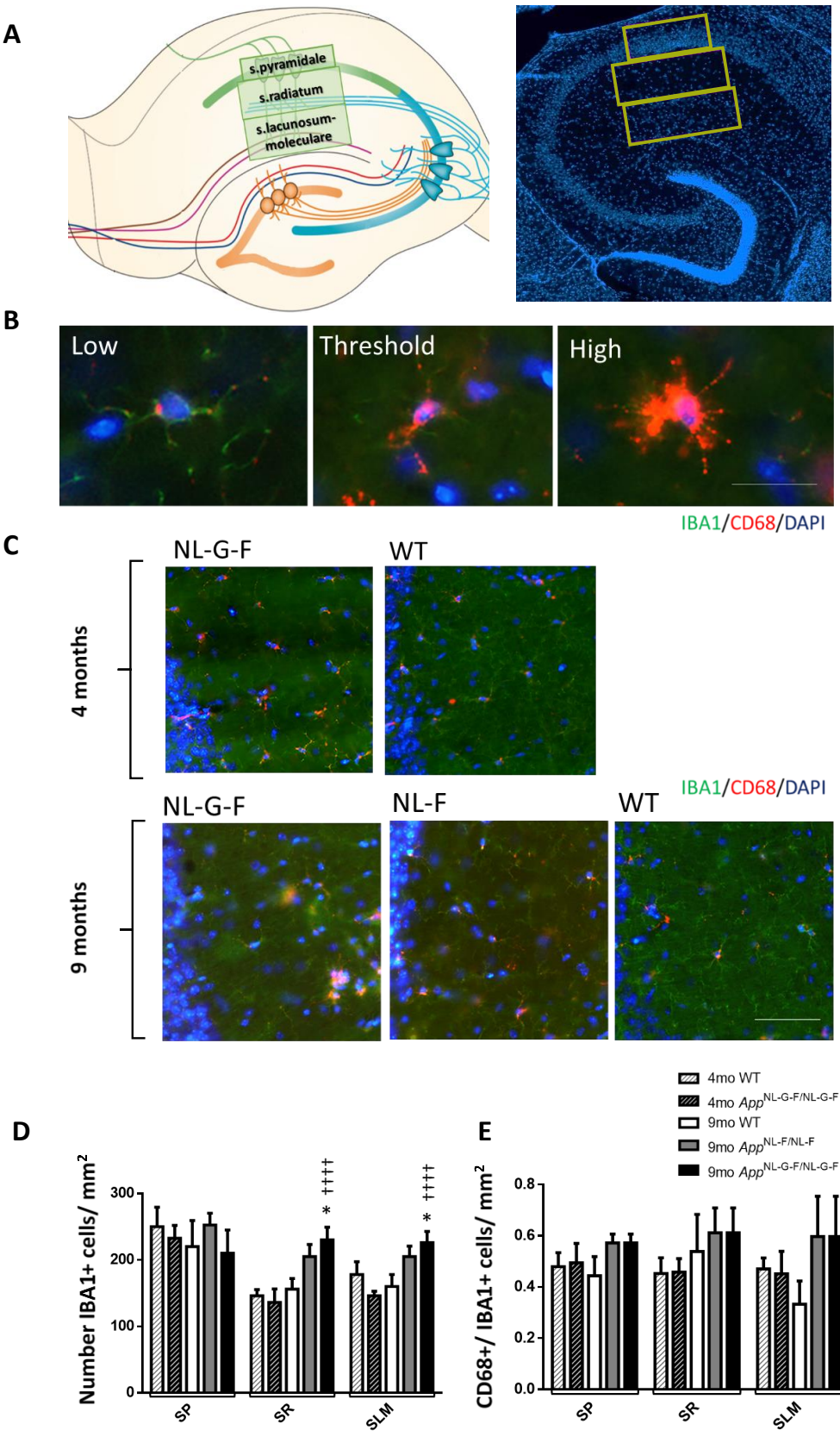
A
s.pyramidale
s.radiatum
s.lacunosum-moleculare
B
Low
Threshold
High
IBA1/CD68/DAPI
C
NL-G-F
WT
4 months
IBA1/CD68/DAPI
NL-G-F
NL-F
WT
9 months
D
Number IBA1+ cells/ mm2
300
200
100
0
SP
SR
SLM
E
CD68+/ IBA1+ cells/ mm2
0.8
0.6
0.4
0.2
0.0
4mo WT
4mo App NL-G-F/NL-G-F
9mo WT
9mo App NL-F/NL-F
9mo App NL-G-F/NL-G-F

Figure 1. Microglial numbers are significantly increased in the CA1 of *App*$^{NL-G-F/NL-G-F}$ mice at 9-months, but not at 4-months.

(A) Diagram (left) and brain slice from wildtype mouse, stained with DAPI (right), to show how sub-regions of CA1 were marked to be counted. Microglia were counted in the SLM and SR, in marked boxes of area 100,000µm^2 and in the SP in marked box of area 40,000 µm^2.
(B) Images, taken with EVOS® FL Auto-Cell Imaging System, representing threshold levels for CD68 detection. Cells were CD68 positive if more than 30% of their cell body contained red fluorescence (threshold and high). Scale= 20µm.
(C) Representative images of hippocampal regions from 4- and 9-month *App*-KI and wildtype mice, stained with IBA1 (green) and CD68 (red) and imaged with the EVOS® FL Auto-Cell Imaging System. Scale= 40µm.
(D) Highly significant interaction of age and genotype within sub-region for density of microglial/IBA1+ cells ($p<0.0001$, GLMM). Significantly higher numbers of IBA1+ cells were observed in the SLM and SR of *App*$^{NL-G-F/NL-G-F}$ mice at 9-months compared to WT controls ($p<0.05$, sequential Sidak) and compared to 4-month *App*$^{NL-G-F/NL-G-F}$ mice ($p<0.0001$).
(E) Highly significant interaction of age and genotype within region for the proportion of CD68+ cells in the total microglial population (IBA1+ cells) ($p<0.0001$, GLMM). Sequential Sidak test revealed no significant differences between groups.

N=5 mice per group. Data shown as Mean±SEM. GLMM (age x genotype within region) and sequential Sidak tests, if there was a significant interaction. † and * symbols show significant pairwise comparisons of *App*$^{NL-G-F/NL-G-F}$ mice ages and 9-month *App*$^{NL-G-F/NL-G-F}$ compared to 9-month WT respectively, *$p<0.05$, ††††$p<0.0001$. SP= stratum pyramidale, SR= stratum radiatum, SLM= stratum lacunosum-moleculare.

To further understand the activity profile of microglia in these *App*-KI models, Major histocompatibility Class II (MHC-II) expression, was investigated by immunohistochemistry. MHC-II is primarily expressed on microglia in the brain and is a marker of microglial activation, although it may also be expressed at low levels on surveillance cells (Hopperton et al., 2018). Microglia present foreign antigens on their cell surface, bound to MHC-II molecules (Perlmutter et al., 1992). Hemispheres, fixed by immersion in 4% paraformaldehyde, of brains from *App*-KI mice and WT controls at 9-months and 4-months were co-stained with IBA1 and MHC-II. Double positive (IBA1+ and MHC-II+) microglia in sub-regions of CA1 and CA3 of hippocampus were quantified from images taken on the EVOS® FL Auto-Cell Imaging System. The CA3 was also quantified here because, upon imaging the whole hippocampus this area appeared to have a high concentration of double positive cells. As CA3 receives input from the EC and sends projections to CA1 it is also an area of interest, as it is affected by pathology and neurodegeneration in the early stages of AD (Braak et al., 2006; Thal et al., 2002). There was a significant interaction between age and genotype for double positive microglial counts within these hippocampal sub-regions ($p<0.0001$, GLMM, n=4-5 animals per group; Figure 2B). Surprisingly, there were almost no, or absolutely no MHC-II positive cells detected in any group or region except for in 9-month *App*$^{NL-G-F/NL-G-F}$ mice. Here a subset of

the total population of microglia (IBA1+ cells), in every sub-region, clearly expressed MHC-II ($p<0.0001$ for 9-month *App*$^{NL-G-F/NL-G-F}$ compared to 9-month WT, 9-month *App*$^{NL-F/NL-F}$ and 4-month *App*$^{NL-G-F/NL-G-F}$, sequential Sidak, n=4-5 animals per group; Figure 2B). This suggests that microglia in the 9-month *App*$^{NL-G-F/NL-G-F}$ mice show a strong phenotype of antigen presentation in response to the well-developed amyloid plaques at 9-months, but not as plaques first start developing at 4-months of age.

A

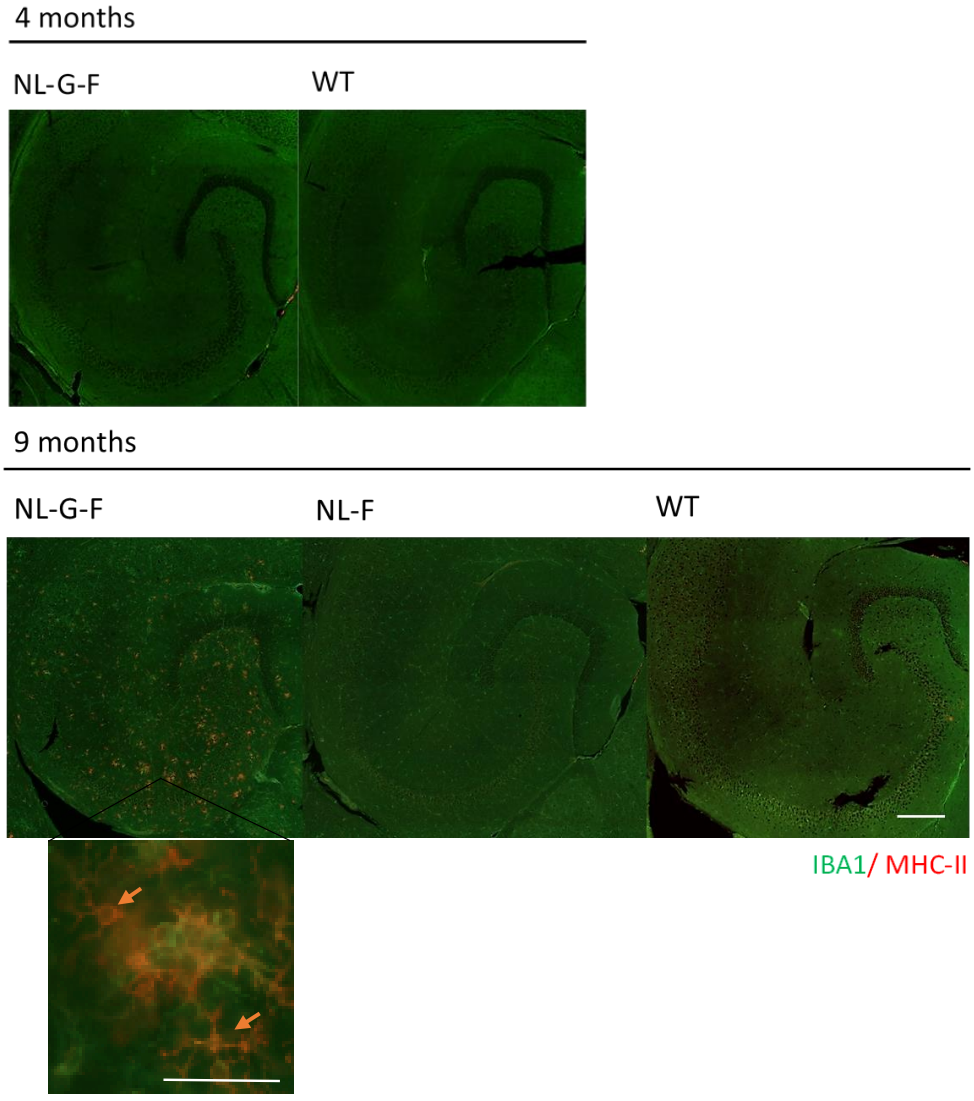
4 months
NL-G-F
WT
9 months
NL-G-F
NL-F
WT
IBA1/ MHC-II

B

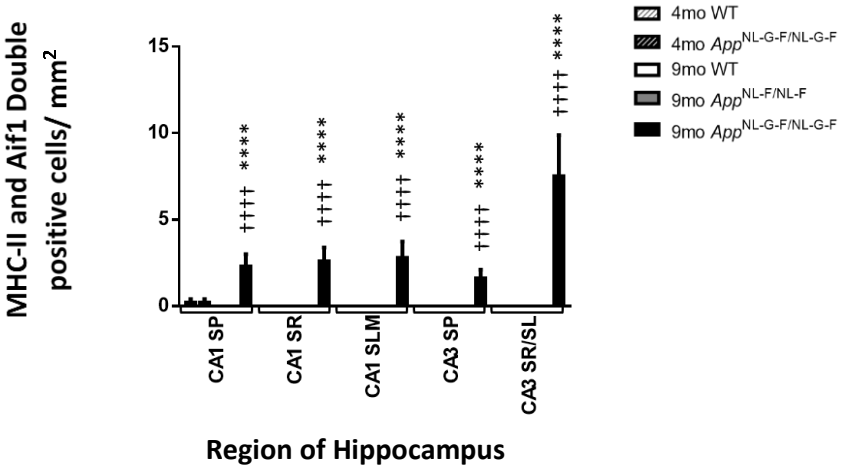
MHC-II and Aif1 Double positive cells/ mm2
15
10
5
0
CA1 SP
CA1 SR
CA1 SLM
CA3 SP
CA3 SR/SL
Region of Hippocampus
4mo WT
4mo App NL-G-F/NL-G-F
9mo WT
9mo App NL-F/NL-F
9mo App NL-G-F/NL-G-F

Figure 2. MHC-II positive microglial cells in the hippocampus increases in 9-month *App*$^{NL-G-F/NL-G-F}$ mice compared to, WT controls, *App*$^{NL-F/NL-F}$ and 4-month *App*$^{NL-G-F/NL-G-F}$ mice.

(A) Representative images of hippocampal regions from 4- and 9-month *App*-KI and wildtype mice, stained with IBA1 (green) and MHC-II (red) and imaged with the EVOS® FL Auto Cell Imaging System. Scale= 200µm. Inset show MHC-II positive cells with arrows for 9-month *App*$^{NL-G-F/NL-G-F}$. Scale=20 µm.

(B) A highly significant interaction for double positive (MHC-II+ and IBA1+) cells was seen within each sub-region of CA1 and CA3 counted (GLMM, $p<0.0001$). Double positive cells were observed in all hippocampal regions counted in 9-month *App*$^{NL-G-F/NL-G-F}$ mice, whereas no or almost no double positive microglia were seen in any other groups ($p<0.0001$ 9-month *App*$^{NL-G-F/NL-G-F}$ compared to 9-month WT, 9-month *App*$^{NL-F/NL-F}$ and 4-month *App*$^{NL-G-F/NL-G-F}$ mice, sequential Sidak).

N=5 mice per group, except for 9-month *App*$^{NL-F/NL-F}$ for which n=4 mice. Data shown as Mean±SEM. GLMM (age x genotype within region) followed by sequential Sidak test. † and * symbols show significant pairwise comparisons of ages of *App*$^{NL-G-F/NL-G-F}$ mice and 9-month *App*$^{NL-G-F/NL-G-F}$ compared to 9-month WT respectively, † † † † /**** $p<0.0001$. CA3: SP= stratum pyramidale, SR= stratum radiatum, SL= stratum lucidum.

Expression of microglial genes involved in proliferation and activation in the cerebral cortex differ with the presence of amyloid pathology

To further address the question of how amyloid pathology affects microglial proliferation and activity, the expression levels of general microglial marker genes (*Aif1 and Spi1*) and markers of microglial activity (*Cd68, H2ab1, C1qa* and *Csf1r*) were quantified by reverse transcriptase quantitative PCR (RT-qPCR), in the cortex of 9-month *App*$^{NL-G-F/NL-G-F}$ vs WT controls. The cerebral cortex was selected for investigation as it is among one of the earliest areas in which amyloid pathology is observed (Thal et al., 2002) and functions associated with the cortex are impaired in AD. *Aif1* encodes IBA1 (described above) and *Spi1* encodes the transcription factor PU1. These genes have been selected as general microglial markers because they are constitutively expressed by microglia, independent of the microglial activation state, and are necessary for microglial function and viability (Ito et al., 1998; Smith et al., 2013; Walton et al., 2000). Expression levels of *Aif1* cDNA were normalised between genotypes by comparing to expression levels of housekeeping gene, *Rps28*. RT-qPCR revealed *Aif1* expression, normalised to *Rps28*, is not significantly different in *App*$^{NL-G-F/NL-G-F}$ mice compared to WT controls (Figure 3A). Surprisingly, this differs to results obtained by immunohistochemistry in the hippocampus. It is important to consider that cortical cDNA used for RT-qPCR was generated from RNA from the whole mouse cortex, and thus includes all cell types, including astrocytes, neurons and microglia. These other cell types can dilute the signal from the RT-qPCR. Also, gene expression differs between genotypes and could be due to changes in total microglial numbers, rather than altered gene expression per microglial cell. To account for this, *Aif1* expression levels were used as a reference for total microglial numbers, and all other

gene expression levels were analysed as a ratio of *Aif1* expression levels, to understand the differences in gene expression within microglial cells. All the following genes tested by RT-qPCR, and normalised to *Aif1* expression, were analysed together in a repeated measures 2-way ANOVA, as the 11 different candidate genes were tested in the same mice. Overall, there were significant main effects of both candidate gene tested by RT-qPCR and mouse genotype ($p<0.0001$ and $p<0.01$ respectively) and a highly significant interaction ($p<0.0001$). The apparent trend in *Spi1* expression was not significant ($p=0.12$, Sidak's *post-hoc* test after a significant interaction with repeated measures two-way ANOVA, n=6-8 animals per group; Figure 3B). A larger sample size would be needed to assess whether this is a real difference.

Figure 3. General microglial marker gene transcripts, in 9-months *App*$^{NL\text{-}G\text{-}F/NL\text{-}G\text{-}F}$ mice cortex compared to WT controls.

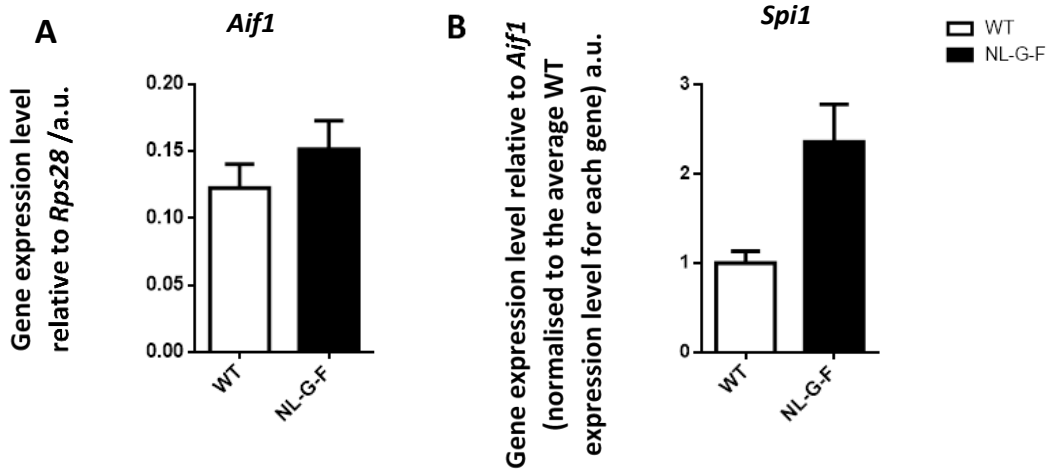

(A) *Aif1* expression was not significantly different in 9-month *App*$^{NL\text{-}G\text{-}F/NL\text{-}G\text{-}F}$ compared to WT controls, as measured by RT-qPCR, and normalized to housekeeping gene *Rps28*.

(B) *Spi1* expression levels, measured by RT-qPCR, was plotted relative to *Aif1* and normalised to the average WT expression. *Spi1* showed a tendency for increase in 9-month *App*$^{NL\text{-}G\text{-}F/NL\text{-}G\text{-}F}$ compared to WT controls ($p=0.12$).

N=6 WT and n=8 *App*$^{NL\text{-}G\text{-}F/NL\text{-}G\text{-}F}$ mice. Data shown as Mean±SEM. *Aif1:* Unpaired two-tailed Students *t*-test. *Spi1*: Two-way repeated measures ANOVA for 11 candidate genes tested by RT-qPCR in the same mice, followed by Sidak's *post-hoc* test as there was a significant interaction between candidate gene tested by RT-qPCR and mouse genotype.

The following genes have been selected to investigate microglial activity changes in response to amyloid pathology, as they are expressed by microglia in a variety of activity states. *Cd68* encodes CD68 (discussed above), *H2ab1* encodes a subunit of MHC-II, *C1qa* encodes Complement C1q subcomponent subunit A, which is a constituent of the first component of the complement system and *Csf1r* encodes Colony stimulating factor 1 receptor. Microglia are

the dominant source of C1q in the mouse brain and C1q in involved in recognising and responding to pathogens or debris in the local environment (Fonseca et al., 2017). MHC-II is involved in antigen presentation (Perlmutter et al., 1992) and the CSF-1R in microglial survival (Elmore et al., 2014). RT-qPCR revealed *Cd68* and *H2ab1* gene expression was significantly increased by approximately 3-fold in *App*$^{NL\text{-}G\text{-}F/NL\text{-}G\text{-}F}$ mice compared to WT controls ($p<0.01$ and $p<0.001$ respectively, Sidak *post-hoc* tests, n=6-8 animals; Figure 4). Expression levels of *C1qa* and *Csf1r* relative to *Aif1* were not significantly different between genotypes (Figure 4). Overall, these data suggest antigen presentation and phagocytotic activity of microglia is increased in *App*$^{NL\text{-}G\text{-}F/NL\text{-}G\text{-}F}$ mice compared to controls, in response to amyloid pathology.

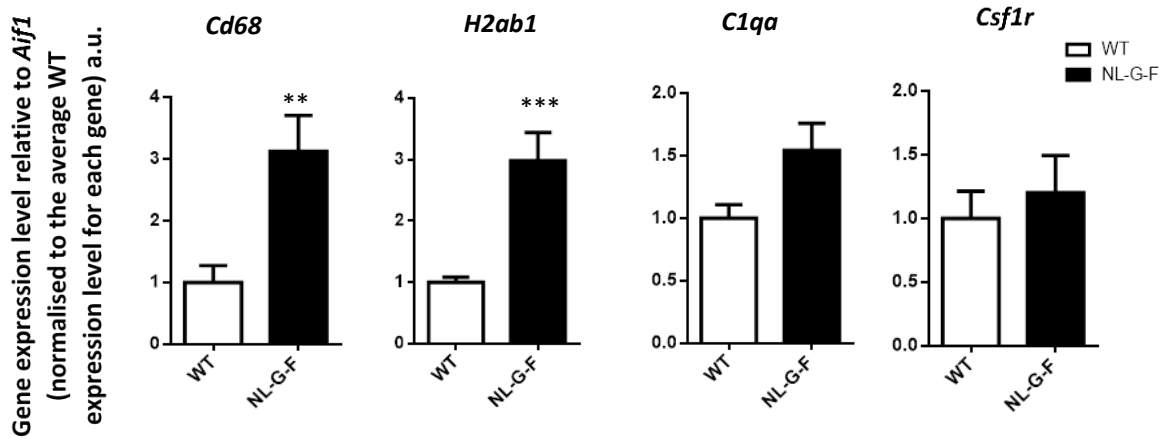

Figure 4. Microglial gene transcripts associated with activation of specific functions, in 9-months *App*$^{NL\text{-}G\text{-}F/NL\text{-}G\text{-}F}$ mice cortex compared to WT controls.

Significant increases were seen in *Cd68* and *H2ab1* expression in 9-month *App*$^{NL\text{-}G\text{-}F/NL\text{-}G\text{-}F}$ compared to WT controls ($p<0.01$ and $p<0.001$ respectively, Sidak's *post-hoc* tests). *C1qa* and *Csf1r* expression were not significantly different between genotypes. Expression levels measured by RT-qPCR, plotted relative to *Aif1* and normalised to the average WT expression.

N=6 WT and n=8 *App*$^{NL\text{-}G\text{-}F/NL\text{-}G\text{-}F}$ mice. Data shown as Mean±SEM. Repeated measures two-way ANOVA followed by Sidak's *post-hoc* test as there was a significant interaction (described in legend to Figure 3), *post-hoc* test significance marked above individual groups, ** $p<0.01$, ***$p<0.001$.

Gene expression of microglial inflammatory and GWAS gene transcripts differ with the presence of amyloid pathology in the cerebral cortex

Changes in the expression levels of pro- and anti-inflammatory microglial genes, and genes identified by GWAS to be risk factors for AD, were investigated by RT-qPCR in the cortex of 9-month *App*$^{NL\text{-}G\text{-}F/NL\text{-}G\text{-}F}$ mice compared to WT controls. The GWAS genes: *Trem2,* encoding triggering receptor expressed on myeloid cells*; Abi3,* encoding ABI gene family member 3 and *Plcg2,* are highly expressed in microglia*. Trem2* is involved in mediating phagocytic clearance

of apoptotic cell debris (Kleinberger et al., 2014) and variants are strong risk factors for AD (Guerreiro et al., 2013; Jonsson et al., 2013; Sims et al., 2017). *Plcg2* is a transmembrane signalling enzyme involved in transmitting signals from immune system receptors across the cell membrane and a protective variant has been found in AD (Sims et al., 2017). Abi3 encodes ABI gene family member 3, a transcription factor regulating actin polymerization, and a variant that modifies risk of AD has been found (Sims et al., 2017). RT-qPCR demonstrated *Trem2* expression relative to *Aif1* expression was significantly increased, almost 5-fold, in the cortex of *App*$^{NL\text{-}G\text{-}F/NL\text{-}G\text{-}F}$ mice compared to WT controls ($p<0.0001$, Sidak's *post-hoc* test, n=6-8 animals). Interestingly, *Plcg2* and *Abi3* expression were not significantly different between genotypes (Figure 5), suggesting that different risk genes for AD behave differently in response to amyloid pathology in the *App*$^{NL\text{-}G\text{-}F/NL\text{-}G\text{-}F}$ mice.

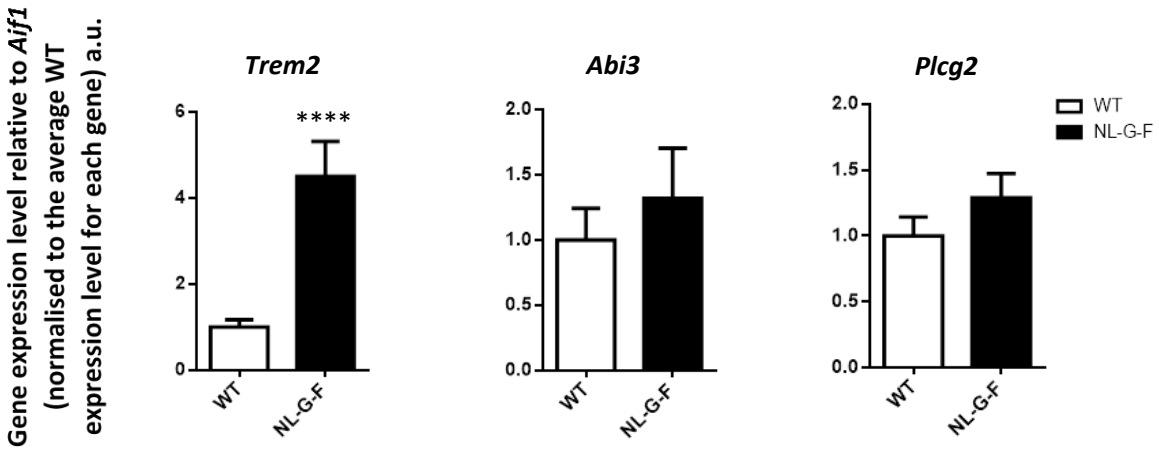

Figure 5. Microglial gene transcripts for risk genes for AD identified by GWAS, in 9-months *App*$^{NL\text{-}G\text{-}F/NL\text{-}G\text{-}F}$ mice cortex compared to WT controls.

A significant increase in *Trem2* expression was seen in 9-month *App*$^{NL\text{-}G\text{-}F/NL\text{-}G\text{-}F}$ compared to WT controls ($p<0.0001$, Sidak's *post-hoc* test). *Plcg2* and *Abi3* expression were not significantly different between genotypes. Expression levels measured by RT-qPCR, plotted relative to *Aif1* and normalised to the average WT expression

N=6 WT and n=8 AppNL-G-F/NL-G-F mice. Data shown as Mean±SEM. Repeated measures two-way ANOVA followed by Sidak's *post-hoc* test as there was a significant interaction (described in legend to Figure 3), *post-hoc* test significance marked above individual groups, ****$p<0.0001$.

To understand changes in polarity of microglia, markers associated with either pro- or anti-inflammatory microglial phenotypes were investigated. The pro-inflammatory marker gene *Tnf*, encoding tumour necrosis factor alpha, one of the classical pro-inflammatory cytokines involved in microglial activation in a proinflammatory direction (Kuno et al., 2005), was investigated. Three marker genes involved in the anti-inflammatory microglial phenotype were

also studied: *Arg1*, encoding Arginase-1*, Tgfβ,* encoding the classical anti-inflammatory cytokine transforming growth factor beta 1 and *Mrc1,* encoding mannose receptor C type-1 (Cherry et al., 2014). RT-qPCR demonstrated there were no significant differences in expression levels of anti-inflammatory (*Arg1*, *Mrc1* and *Tgfβ)* or pro-inflammatory (*Tnf*) genes, relative to *Aif1* expression (Figure 6). Overall, these data suggest that the pro- and anti-inflammatory polarisation of microglia is not altered in the *App*$^{NL\text{-}G\text{-}F/NL\text{-}G\text{-}F}$ mice from the canonical genes tested here, indicating that it is likely TREM2-related cellular processes, and specific functions of microglia such as phagocytosis and antigen presentation that are altered in microglia in these mice.

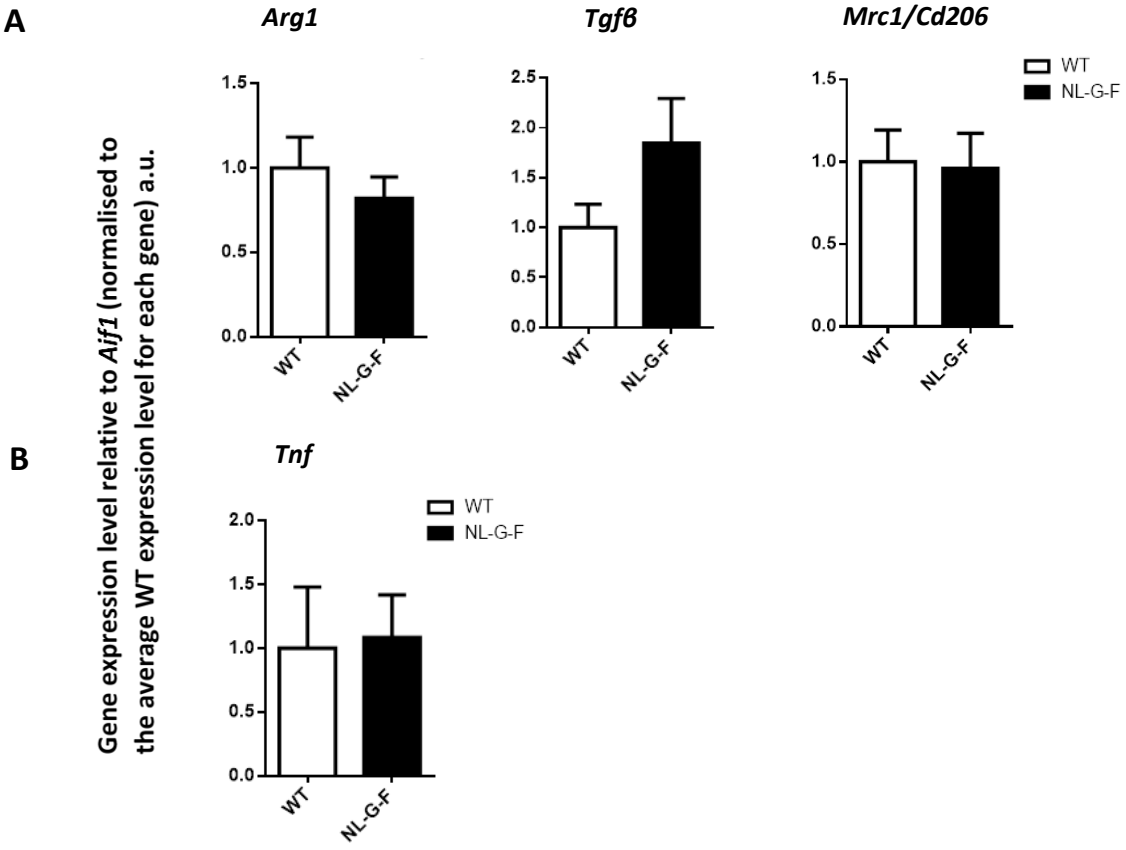

Figure 6. Microglial anti-inflammatory and pro-inflammatory gene transcripts in the cortex of 9-months *App*$^{NL\text{-}G\text{-}F/NL\text{-}G\text{-}F}$ mice compared to WT controls.

(A) There were no significant differences in expression levels of anti-inflammatory genes (*Arg1, Tgfβ, Mrc1*) in 9-month *App*$^{NL\text{-}G\text{-}F/NL\text{-}G\text{-}F}$ compared to WT controls.
(B) There was no significant increase in pro-inflammatory gene, *Tnf,* expression in 9-month *App*$^{NL\text{-}G\text{-}F/NL\text{-}G\text{-}F}$ compared to WT controls.

Expression levels of A and B measured by RT-qPCR, plotted relative to Aif1 and normalised to the average WT expression. N=6 WT and n=8 *App*$^{NL\text{-}G\text{-}F/NL\text{-}G\text{-}F}$ mice. Data shown as Mean±SEM. Repeated measures two-way ANOVA followed by Sidak's *post-hoc* test as there was a significant interaction (described in legend to Figure 3).

DISCUSSION

Microglial proliferation changes in the hippocampus with amyloid pathology in *App*-KI mice

Here, we report that total microglial number and proportion of phagocytic microglia, within sub-regions of CA1, is affected by amyloid pathology in the *App*-KI mice. The *App*$^{NL\text{-}G\text{-}F/NL\text{-}G\text{-}F}$ mice showed significant increases in microglial numbers in the SR and SLM at 9-months by immunohistochemistry, consistent with developed amyloid pathology. These findings are similar to previous findings in our lab in *APP*^{Swe} overexpression mice (Liu, 2017). Immunohistochemistry results in human brain tissue in patients diagnosed with AD also show significantly higher numbers of microglia (Olmos-Alonso et al., 2016). Moreover, microglial gene expression in amyloid mice was found to be correlated with plaque load almost 1:1 (Matarin et al., 2015), and a correlation between Aβ plaques and microglial response has also been previously reported in *App*$^{NL\text{-}G\text{-}F/NL\text{-}G\text{-}F}$ mice (Castillo et al., 2017). These results together strongly suggest microglia proliferation in response to Aβ plaques. In this way it is perhaps surprising that we report no change in microglial numbers in the 4-month *App*$^{NL\text{-}G\text{-}F/NL\text{-}G\text{-}F}$ mice, where plaques are present. Conversely, in App$^{NL\text{-}F/NL\text{-}F}$ mice, where at 9-months plaques are very minimal with only a small number observed in the cortex, microglia show a tendency for being increased compared to WT controls, which is close to significance level. One possibility which would account for these findings is that deposited Aβ plaques are not the primary signal for microglial proliferation. A signal must differ between the App$^{NL\text{-}F/NL\text{-}F}$ and *App*$^{NL\text{-}G\text{-}F/NL\text{-}G\text{-}F}$ strains, causing their microglial proliferation to occur at different stages in amyloid pathology progression. It is important to note that Aβ species, can be both soluble and insoluble, and occur in various aggregation states. Human and animal model evidence implicates soluble toxic Aβ aggregates, and not plaques, as the key driver of neurodegeneration and cognitive decline in AD patients (Esparza et al., 2013; Hong et al., 2016; Shankar et al., 2008). *In vitro*, soluble Aβ seems to interact with cultured microglia via their scavenger-A receptor and can activate microglia even at very low (nanomolar) concentrations (Maezawa et al., 2011). However, it is not clear to what extent this represents microglial responses *in vivo* in the brain, where they are part of a complex 3D environment, by which they are finely regulated. Furthermore, the process of isolating microglia from the brain to culture them, may cause them to become activated and undergo morphological and gene expression changes. It is possible that the App$^{NL\text{-}F/NL\text{-}F}$ mice have more soluble Aβ in the hippocampus at an earlier stage compared to the *App*$^{NL\text{-}G\text{-}F/NL\text{-}G\text{-}F}$ mice. The Arctic mutation, in the *App*$^{NL\text{-}G\text{-}F/NL\text{-}G\text{-}F}$ mice, which makes Aβ more prone to aggregate (Tsubuki et al., 2003), may result in a shift of the equilibrium of soluble Aβ and insoluble Aβ (in plaques), so more soluble Aβ is buffered into

plaques. Consequently, amyloid pathology may need to be more advanced before soluble Aβ aggregates will be present in the hippocampus at a sufficient concentration to be released from plaques into the extracellular space, stimulating microglial proliferation in the *App*$^{NL\text{-}G\text{-}F/NL\text{-}G\text{-}F}$ mice. Also, interestingly, microglial proliferation was not seen in the SP. A possible explanation for this is that there might be a lower concentration of soluble aggregates in this sub-region of CA1. This is consistent with the idea of Aβ being released from glutamatergic synapses (Revett et al., 2013), of which there are less of in SP compared to other layers, as this mainly contains cell bodies.

IBA1, encoded by Aif1, is a cytoplasmic protein involved in actin cross-linking (Ohsawa et al., 2004). Interestingly, *Aif1* expression in a microarray in amyloid mice was very dependent on the stage of amyloid pathology, appearing several months following first deposition and with our immunohistochemistry results this suggests the *App*$^{NL\text{-}G\text{-}F/NL\text{-}G\text{-}F}$ mice display an increase in IBA1 in the hippocampus later than expected compared to other amyloid mice (Matarin et al., 2015). Here, we report no significant difference in the relative expression of *Aif1* between *App*$^{NL\text{-}G\text{-}F/NL\text{-}G\text{-}F}$ mice and WT controls, measured by RT-qPCR, unlike the increase we saw with immunohistochemistry. The discrepancy of results to the hippocampus, could have several explanations. Firstly, in the hippocampus IBA1-positive cells were being counted, reflecting total microglial number, rather than total *Aif1* expression at the mRNA level. It is possible that within each microglial cell there was less *Aif1* expressed in the *App*$^{NL\text{-}G\text{-}F/NL\text{-}G\text{-}F}$ mice, but overall by RT-qPCR the total *Aif1* expression is not changed between genotypes. This could indicate fragmentation of the cytoskeleton of microglia in *App*$^{NL\text{-}G\text{-}F/NL\text{-}G\text{-}F}$ mice, reflecting altered function, in response to amyloid pathology. Secondly, amyloid pathology may be at different levels of advancement in cortical regions compared to the hippocampus (Thal et al., 2002). Furthermore, RT-qPCR measures mRNA levels of *Aif1* whereas immunohistochemistry labels specific proteins. Perhaps the discrepancy lies in the differential regulation of IBA1 mRNA versus protein, so in this case perhaps transcription rate was not affected, but translation was increased. In this way, it is essential to test the same tissue by RT-qPCR and immunohistochemistry before making firm conclusions. Finally, RT-qPCR was done on whole tissue so perhaps this dilutes the signal too much to reliably detect a change. In addition, my initial power calculations suggest the level of mean difference from the *Aif1* would not be detectable as significant at this sample size (see materials and methods), so a larger sample size for RT-qPCR would be needed to detect smaller differences in mean expression.

Microglial phagocytic activity and antigen presentation increases with amyloid pathology in *App*-KI mice

We also reported by immunohistochemistry a significant interaction between age and genotype, suggesting the proportion of microglia showing lysosomal activity within the sub-regions of CA1 is increased at 9-months in both *App*-KI genotypes, but individual comparisons were not significant. This parallels results from our lab in APP/PSEN1 overexpression mice (Liu, 2017). Additionally, by RT-qPCR we found *Cd68* expression to be increased in $App^{NL\text{-}G\text{-}F/NL\text{-}G\text{-}F}$ mice, by approximately 3-fold compared to WT controls. This is in line with human post-mortem results, where the level of dementia is positively correlated with CD68 expression (Minett et al., 2016), suggesting the upregulation of phagocytic activity by microglial in response to amyloid pathology. However, this could also be in part due to response to other aspects of the disease such as tau tangles or neuronal loss, which occur at a later stage in the disease than the *App*-KI mice represent. Our results also correspond to findings in a transgenic AD mouse model, in which CD68-positive microglia gather around injected Aβ and reduce its levels over time (Matsumura et al., 2015). However, in this case as the Aβ was an exogenous added substance, this could have caused a different response of microglia than they would have to endogenous Aβ. In fact, studies depleting microglia observed no differences in amyloid plaque load (Dagher et al., 2015; Olmos-Alonso et al., 2016). This suggests the primary role of phagocytic microglia is not to clear amyloid plaques. Instead, they may clear dystrophic neurites (Hong et al., 2016), as they release soluble Aβ in AD. The discrepancy in lack of significance between 9-month $App^{NL\text{-}G\text{-}F/NL\text{-}G\text{-}F}$ mice and WT mice in the immunohistochemistry might be explained by different levels of amyloid pathology between the cortical and hippocampal regions. In a transgenic AD model, two stages were observed in microglial phenotypes. An earlier stage in which activated microglia were negative for CD68 and a later stage in which they were positive, when pathology was more developed (Matsumura et al., 2015). Another explanation is that in the hippocampus microglia were classified as CD68 positive, if above a certain threshold for CD68 immunofluorescence, but total CD68 fluorescence was not classified, as the immunohistochemistry was done in several batches. It is therefore possible that CD68 levels per microglial cell, were overall increased.

Consistently, by RT-qPCR we report that *Spi1* showed a trend for increase in the $App^{NL\text{-}G\text{-}F/NL\text{-}G\text{-}F}$ mice. Knocking down PU.1 (encoded by *Spi1*) *in vitro* with siRNA, reduces the ability of adult human microglia to phagocytose Aβ1-42 (Smith et al., 2013), implicating *Spi1* expression in increased phagocytic activity of microglia. This is particularly relevant as $Aβ_{1\text{-}42}$ level is high in $App^{NL\text{-}G\text{-}F/NL\text{-}G\text{-}F}$ mice, suggesting $Aβ_{1\text{-}42}$ stimulates microglial phagocytosis in this model.

Additionally, by immunohistochemistry we demonstrate that the proportion of the total microglia population that are MHC-II positive increases with progression of Aβ pathology, only being apparent in the more aggressive *App*$^{NL\text{-}G\text{-}F/NL\text{-}G\text{-}F}$ strain, at 9-months. This is consistent with RT-qPCR results showing that *H2ab1* (encoding a subunit of MHC-II) levels are significantly increased in *App*$^{NL\text{-}G\text{-}F/NL\text{-}G\text{-}F}$ mice, compared to WT controls. MHC-II expression is highly upregulated in microglia in human AD brains, particularly on microglia clustered around Aβ plaques (Itagaki et al., 1989; McGeer et al., 1987; Perlmutter et al., 1992). This suggests that this aspect spans early and later stages of AD. Further investigation by co-staining of $A\beta_{1\text{-}42}$ antibodies is needed to understand if MHC-II expression is more prevalent on microglial surrounding plaques. If this is the case, it suggests microglia are responding to plaques or soluble Aβ being released from plaques or dystrophic neurites around plaques, by presenting antigens on their surface in a complex with MHC-II molecules and initiating a downstream immune response to amyloid pathology. This also fits well with the idea of phagocytic microglial activity being increased, as MHC-II presents antigens taken into immune cells by phagocytosis (Brutkiewicz, 2016). Overall, these results suggest microglia near to plaques take on a phagocytic phenotype, due to activation by receptors. Microglia then phagocytose amyloid species, ingesting them into late endocytic compartments where they are complexed with MHC-II and presented on the microglial cell surface. This also suggests microglia are recognising and responding to amyloid pathology and initiating an immune response, by presenting antigens on their surface.

Trem2 expression is increased 5-fold in the cortex with amyloid pathology in *App*$^{NL\text{-}G\text{-}F/NL\text{-}G\text{-}F}$ mice

TREM2 regulates microglial phagocytosis of debris (Kleinberger et al., 2014) and has been shown to directly bind Aβ and mediate its degradation (Zhao et al., 2018). Previous work in our lab in APP/PSEN1 overexpression models shows a striking increase (6-fold) expression in TREM2 protein, compared to wildtype (WT) controls. *Trem2* formed a hub gene with a network of immune genes, including *Plcg2* and *Abi3*, and microglial genes, including *Aif1* and *Cd68*. The genes were highly correlated (r=0.97) with amyloid, suggesting their expression is upregulated in response to amyloid pathology (Matarin et al., 2015) and therefore suggesting an increase in phagocytic microglia. TREM2 mutations associated with AD were found to reduce the ability of TREM2 to bind and react appropriately to Aβ and impairs Aβ degradation in both primary microglial culture and mouse brain (Zhao et al., 2018), suggesting microglia are involved in clearance of Aβ. In humans, TREM2 levels in the hippocampus peaks in the early stages of AD but drop in the later stages of the disease (Suarez-Calvet et al., 2016). This drop could reflect an increase and subsequent reduction in microglial phagocytic function,

meaning Aβ is cleared less effectively later in the disease. Here, we report a nearly 5-fold increase in *Trem2* expression in the *App*$^{NL\text{-}G\text{-}F/NL\text{-}G\text{-}F}$ mice measured by RT-qPCR, which is not accounted for by an increase in total microglial numbers. This is consistent with previous findings in our lab in *APP* overexpression mice (Liu, 2017; Matarin et al., 2015). Taken together, these results suggest that *Trem2* expression in the *App*$^{NL\text{-}G\text{-}F/NL\text{-}G\text{-}F}$ mice is upregulated in microglia in response to amyloid pathology, early in AD. This upregulation likely reflects an increase in phagocytic activity and Aβ clearance, which is consistent with the increased expression we see of other genes associated with phagocytosis (*Cd68, H2ab1*). Interestingly, we did not see increases in the other GWAS gene, *Abi3* and *Plcg2*, suggesting *Trem2* is regulated differently to Abi3 and Plcg2, or may be involved in different cellular processes, at least at 9-months in the *App*$^{NL\text{-}G\text{-}F/NL\text{-}G\text{-}F}$ mice.

Inflammatory polarity of microglia in the cortex is not affected by amyloid pathology in *App*$^{NL\text{-}G\text{-}F/NL\text{-}G\text{-}F}$ mice

We report that the presence of amyloid pathology in the cortex of *App*$^{NL\text{-}G\text{-}F/NL\text{-}G\text{-}F}$ mice does not polarise microglia towards canonical pro-inflammatory and anti-inflammatory phenotypes. This is surprising as in AD, reports of increased anti-inflammatory and pro-inflammatory microglial markers have been reported (Wang et al., 2015). However, other results in this study suggest an increase in phagocytic activity of microglia which is more associated with anti-inflammatory microglia (Koenigsknecht-Talboo and Landreth, 2005; Michelucci et al., 2009). The *App*$^{NL\text{-}G\text{-}F/NL\text{-}G\text{-}F}$ mice represent a very early stage in` AD so perhaps more substantial changes to microglial inflammatory phenotypes occur at a later stage in the disease progression, in relation to cell death. In fact, a longitudinal human study revealed two stages of microglial activation, an early protective peak in activation, perhaps associated with phagocytosis, in patient with mild cognitive impairment which then declined, and a second peak, perhaps associated with pro-inflammatory phenotypes, in late stages of AD as amyloid clearance failed (Fan et al., 2017). Correspondingly, a recent study has revealed evidence for specific disease associated microglia which are distinct from classical pro- or anti-inflammatory microglia, having reduced expression of homeostatic microglial genes and an increase in expression of pro-inflammatory molecules (Krasemann et al., 2017). In support of this, microglia associated with plaques have been shown to be hyperreactive to lipopolysaccharide treatment compared to non-plaque associated microglia, suggesting microglia function differently around plaques (Yin et al., 2017). So, it seems likely that in the *App*$^{NL\text{-}G\text{-}F/NL\text{-}G\text{-}F}$ mice, which represent early pre-clinical AD, microglia are acting in a protective way to phagocytose amyloid beta and dystrophic neurites. The results suggest the microglia

show no differences in polarity at this early stage of the disease. In later stages of AD microglia may take on a pro-inflammatory disease like-phenotypes, in response to amyloid pathology and other disease related changes.

In conclusion, this study sheds light on microglial phenotypes in both the hippocampus and the cortex of the *App*-KI models, at cellular and mRNA levels respectively, revealing an increase in microglial proliferation and phagocytic activity in response to well-established amyloid pathology (Figure 7). Microglial dysfunction has been implicated in AD by GWAS and genetic studies, making microglia a potential target for therapeutic intervention in AD. There is now evidence that microglia are protective early in AD progression (Fan et al., 2017; Hamelin et al., 2016), supported by increased phagocytic activity of microglia observed in this study. Therefore, investigating drugs to increase microglial phagocytosis of amyloid pathology at these early stages could provide therapeutic benefit for early disease stages. Techniques to diagnose AD earlier in patients, such as PET scans with Aβ ligands, and genetic screening to identify at risk individuals, are making pre-clinical AD therapies more realistic. Based on our research, *App*-KI models, representing early pre-clinical AD, may provide an invaluable tool in which to explore potential drug targets to increase early protective microglial clearance of Aβ and dystrophic neurites.

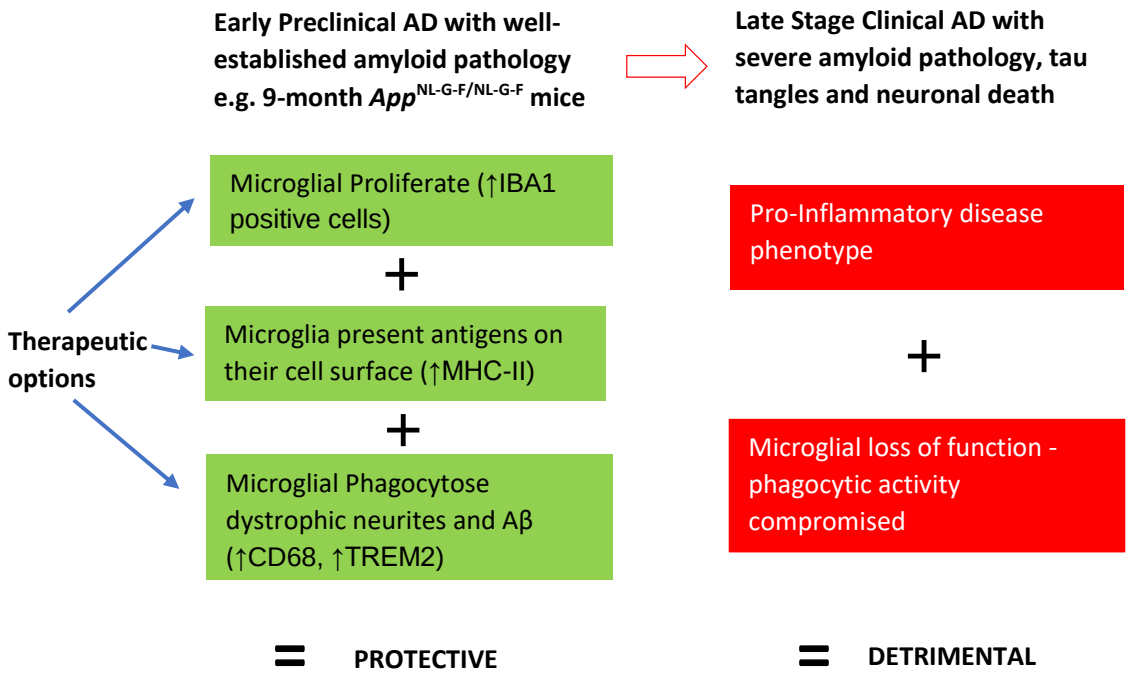

Figure 7. Microglial involvement at early and late stages of AD progression

Microglia act in a protective fashion early in the AD progression, clearing Aβ and dystrophic neurites. Later, microglia take on a distinct pro-inflammatory disease phenotype, promoting

detrimental effects. This study suggests microglial phenotypic changes associated with early disease stages include: microglia proliferation, increased phagocytic activity and antigen presentation. (Original figure).

Limitations

It is important to acknowledge the limitations in this study, to allow for correct interpretation of data. Firstly, for the RT-qPCR, to interpret an increase in gene expression relative to *Aif1* as an increase in that gene's expression for each microglial cell, is an oversimplification. Microglia in the brain are a heterogenous population, with several subgroups with different combinations of gene expression, and functions. In this way, RT-qPCR has limitations in measuring microglial cell gene expression. For example, change in a gene to *Aif1* ratio could also indicate an increased proportion of a subset of the microglia population with substantial expression of that gene, in comparison to other sub-groups of microglia where expression of said gene is relatively low.

Secondly, in results from both RT-qPCR and immunohistochemistry, it is not possible to exclude the possibility that infiltrating macrophages from the periphery are contributing to the results. In human disease, macrophages are not thought to infiltrate substantially into the brain until late stages of the disease and are thought to have distinct phenotypes to resident microglia (Martin et al., 2017). As the *App*-KI mice represent early preclinical stages, we are assuming that infiltrating macrophages are not having a large effect on the results.

There are also considerations in using the *App*-KI models. In both strains, the combination of mutations is not reported to occur together in human AD and so it is not clear if their phenotype is representative of human AD. Moreover, $App^{NL\text{-}G\text{-}F/NL\text{-}G\text{-}F}$ mice have the Arctic mutation in the Aβ sequence, which is not representative of human sporadic AD, in which Aβ has a wildtype sequence. This could produce artefactual results. These limitations need careful consideration when interpreting results, and translating these to human AD.

Future Perspectives

Future research should focus on co-staining microglia for MHC-II and CD68 with plaques, either with thioflavin or an anti-$A\beta_{1\text{-}42}$ antibody, in the hippocampus and the cortex. Microglia can then be quantified within a certain plaque radius, to understand the relation of microglial activation to plaque pathology. Regional differences in plaque load can also be quantified to understand if microglia are responding differently in different brain regions due to different levels of amyloid pathology. RT-qPCR should be carried out in hippocampus to confirm differences in microglial phenotypes from the hippocampus and relate this back to regional

differences in pathology. RNAscope, which measures gene expression in individual cells, should also be employed to confirm changes occurring within individual microglial cells, as opposed to the whole population. Furthermore, new techniques to extract soluble Aβ from the brain (Esparza et al., 2016) or Aβ sequestering antibodies with a high affinity for soluble Aβ (Yamada et al., 2009) could provide useful tools to understand if *App*$^{NL\text{-}F/NL\text{-}F}$ mice have more soluble Aβ at an earlier stage of amyloid pathology than *App*$^{NL\text{-}G\text{-}F/NL\text{-}G\text{-}F}$ mice.

ACKNOWLEDGEMENTS

I would like to thank my supervisors, Professor Frances Edwards and Dr Dervis Salih for their helpful guidance and feedback throughout my project. I would also like to thank Dr Damian Cummings for guidance on my statistical analysis, and Dr Wenfei Lui for the primers used in my RT-qPCR experiments.

STAR★METHODS

Detailed methods include the following:

- KEY RESOURCES TABLE
- EXPERIMENTAL MODEL AND SUBJECT DETAILS
- METHOD DETAILS:
    - Immunohistochemistry
    - Conversion of mRNA to cDNA
    - qRT-PCR
- STATISTICAL ANALYSIS

KEY RESOURCES TABLE

REAGENT OR RESOURCE	SOURCE	IDENTIFIER
Immunohistochemistry		
IBA1	Synaptic Systems	Cat#:234003
CD68	BioRad	Cat#: MCA1957
MHC-II	eBioscience	Cat#: 14-5321
Goat anti-rabbit 488	Jackson ImmunoResearch	Cat#:111-545-144
Goat anti-rat 594	Jackson ImmunoResearch	Cat#:112-585-167
Donkey anti-rabbit 594	Jackson ImmunoResearch	Cat#:711-585-152
Experimental Models		
Transgenic APP^{NL-G-F} mice	Prof Takaomi Saido	N/A
Transgenic APP^{NL-F} mice	Prof Takaomi Saido	N/A
C57BL/6J mice	Originally from The Jackson Laboratory now bred in Edwards Lab.	N/A

Oligonucleotides

Forward Aif*1* Primer	Eurofins Genomics	5'-GGAGACGTTCAGCTACTCTGAC-3'
Reverse *Aif1* Primer	Eurofins Genomics	5'- CATCCACCTCCAATCAGGGC-3'
Forward *Cd68* Primer	Eurofins Genomics	5'- TTCACCTTGACCTGCTCTCTC-3'
Reverse *Cd68* Primer	Eurofins Genomics	5'- GTAGGTTGATTGTCGTCTGCG-3'
Forward *H2ab1* Primer	Eurofins Genomics	5'- AGCTTATTAGGAATGGGGACTGG-3'
Reverse *H2ab1* Primer	Eurofins Genomics	5'-CCGAGGAAGATCACCCCAAG-3'
Forward *Rps28* Primer	Eurofins Genomics	5'-ATCAAGCTGGCTAGGGTAACC-3'
Reverse *Rps28* Primer	Eurofins Genomics	5'-GGCCTTTGACATTTCGGATGA-3'
Forward *Csf1r* Primer	Eurofins Genomics	5'-GGATGGATACCAAATGGCCC-3'
Reverse *Csf1r* Primer	Eurofins Genomics	5'-ACTGGTAGTTGTTAGGCTGC-3'
Forward *Tgfβ* Primer	Eurofins Genomics	5'-ATACCAACTATTGCTTCAGCTCC-3'
Reverse *Tgfβ* Primer	Eurofins Genomics	5'-CAGAAGTTGGCATGGTAGCCC-3'
Forward *Tnfα* Primer	Eurofins Genomics	5'-ACCACGCTCTTCTGTCTACTG-3'
Reverse *Tnfα* Primer	Eurofins Genomics	5'-CAGGCTTGTCACTCGAATTTTG-3'
Forward *Spi1* Primer	Eurofins Genomics	5'-TATCAAACCTTGTCCCCAGCC-3'
Reverse *Spi1* Primer	Eurofins Genomics	5'-TGGTAGGTCATCTTCTTGCGG-3'
Forward *C1qa* Primer	Eurofins Genomics	5'-GTCTCAAAGGAGAGAGAGGGGAG-3'
Reverse *C1qa* Primer	Eurofins Genomics	5'-TATGGACTCTCCTGGTTGGTG-3'
Forward *Abi3* Primer	Eurofins Genomics	5'-CTGTCTCGCAAGAGCATAAAGG-3'
Reverse *Abi3* Primer	Eurofins Genomics	5'-CGGGGTTACAGGTGCTACAG-3'
Forward *Trem2* Primer	Eurofins Genomics	5'-GACCTCTCCACCAGTTTCTCC-3'
Reverse *Trem2* Primer	Eurofins Genomics	5'-TCAGAGTGATGGTGACGGTTC-3'
Forward *Plcg2* Primer	Eurofins Genomics	5'-CTGTGAGATGAGGCCAG TCC-3'
Reverse *Plcg2* Primer	Eurofins Genomics	5'-GTGCGTGTCGTAAAGGA AGAG-3'
Forward *Mrc1* Primer	Eurofins Genomics	5'-GATCCCTCTGGTGAACGGAATG -3'
Reverse *Mrc1* Primer	Eurofins Genomics	5'-GGCACCTATCACAATCAGGAGG -3'
Forward *Arg1* Primer	Eurofins Genomics	5'-ACCTGGCCTTTGTTGATGTCC-3'
Reverse *Arg1* Primer	Eurofins Genomics	5'-CTGGTTGTCAGGGGAGTGTTG-3'

Software and Websites

CFX96 Manager™ Software	BioRad	N/A
Primer-BLAST (NCBI)	https://www.ncbi.nlm.nih.gov/tools/primer-blast/	N/A
Ensembl	http://www.ensembl.org	N/A
GraphPad Prism 6.2	N/A	N/A
IBM Statistics 25 SPSS	N/A	N/A
Adobe Photoshop	N/A	N/A
EVOS® FL Auto Cell Imaging System Software	N/A	N/A
ChemiDoc MP imaging system	Bio-Rad	N/A

EXPERIMENTAL MODEL AND SUBJECT DETAILS

App-KI mouse models were used for this experiment, where the Aβ protein is humanised and human familial AD mutations are inserted (Saito et al., 2014).The humanised *APP* gene is expressed under control of the endogenous murine *App* promoter, ensuring cell specific expression and time of expression remains appropriate in the mouse. Human familial mutations in *APP* are present in the gene. By not overexpressing the *APP* gene by several-fold, *App*-KI models avoid overexpression artefacts or artificial phenotypes associated with expression from an artificial promoter or the influence of random insertion into the mouse genome. The $App^{NL\text{-}F/NL\text{-}F}$ mice have the Swedish (KM670/671NL) mutation, which increases the total levels of Aβ40 and Aβ42 and the Beyreuther/Iberian (I716F) mutation which elevates the Aβ42 to Aβ40 ratio. The $App^{NL\text{-}G\text{-}F/NL\text{-}G\text{-}F}$ mice offer an accelerated model, harbouring the Arctic (E693G) mutation, which promotes Aβ aggregation (by facilitating oligomerization and reducing proteolytic degradation), in addition to the two mutations above (Saito et al., 2014). Homozygous male mice of 4-months and 9-months were used for the present study, except for one homozygous 9-month female mice used for immunohistochemistry. Mice were group-housed in the Biology Services Unit of University College London, with a 12-hour light/dark cycle, with *ad libitum* access to food and water. Age matched wildtype C57BL/6J mice (Jackson Laboratory), housed under the same conditions were used as controls. All procedures were performed in accordance with the United Kingdom Animals (Scientific Procedures) Act 1986.

METHOD DETAILS

Immunohistochemistry

(A) Preparation

Mice were decapitated, and their brains rapidly removed and hemisected on ice. Half the brain was prepared for immunohistochemistry. This was fixed in 4% paraformaldehyde in phosphate buffered saline (PBS) for 24 hours at 4°C, before being transferred to 30% sucrose, 0.03% NaN3 in PBS and stored at 4°C. Using an SM 2000-R microtome (Leica), 30µm transverse sections were cut from each brain and subsequently stored in 0.03% NaN3 PBS at 4°C. At least 3 sections were from the middles of the hippocampus were selected for immunohistochemistry, to allow one spare in case the sections were damaged/torn during the process.

(B) Antibody Staining

Free floating sections were washed in PBS and then permeabilized in 0.3% Triton-X in PBS three times, blocking (3% Goat Serum in 0.3% Triton X-100 in PBS) for 1 hour at room temperature. The sections were then incubated with primary antibodies (see Key Resources Table for details) diluted to 1:400 in blocking solution, overnight at 4°C. Sections were then washed in 0.3% Triton X-100 in PBS three times. They were then incubated for 2 hours at room temperature, with the corresponding Alexa-conjugated secondary antibodies (see Key Resources Table for Details) diluted to 1:800 in blocking solution. The plate was protected from the light to avoid bleaching the fluorophores. The sections were subsequently washed in PBS. The nuclei were counterstained with 4',6-diamidino-2-phenylindole (DAPI 1:10000 in PBS) for 5 minutes. Sections underwent a final wash in PBS. The Sections were mounted on to SuperFrost Plus glass slides (Fisher) with Fluoromount-G medium (Southern Biotech) and left to dry in the dark. Slides were stored at 4°C until they could be analysed.

(C) Imaging and cell counting

Two sections per animal were imaged and analysed, to minimise any image to image variation. Images were taken using the EVOS® FL Auto Cell Imaging System (Life Technologies). The 20X objective was used to image the whole hippocampus, by area defined serial scanning and a motorised stage. To avoid variation between images, the same exposure and brightness settings were used for each image. Images were analysed using Adobe Photoshop software. For IBA1 and CD68 staining, cells were counted in the CA1: stratum radiatum and stratum lacunosum-moleculare, in subfields of size 100,000µm^2 pixels and stratum pyramidum in subfields of size 40,000µm^2. Microglial cells were only counted if their cell body could be seen clearly, with at least two processes protruding from this and more than 50% of the cell body

being present in the subfield. CD68 positive cells were characterised by at least 30% of the cell body containing red fluorescence. MHC-II and IBA1 stained double positive cells were counted in the whole CA1 stratum radiatum stratum, lacunosum-moleculare and stratum pydramidum and, in CA3, stratum pyramidum and the stratum radiatum and stratum lacunosum-moleculare combined, as these could not easily be distinguished.

Isolation of mRNA and conversion to cDNA

Tissue from the cortex of 9-month old WT and *App*$^{NL\text{-}G\text{-}F/NL\text{-}G\text{-}F}$ mice was snap frozen and stored at -80°C. Tissue was homogenised using a homogeniser (Qiagen) with a QIAzol RNA lysis reagent (Qiagen). Total RNA was isolated and purified with miRNAeasy columns, following manufacturer's instructions. The quality (purity and concentration) of the obtained mRNA was assessed with a NanoDrop Spectrophotometer (Thermo Scientific).

RNA was then converted to cDNA by treating 2µg of mRNA with Deoxyribonuclease-I (DNase I, Amplification Grade, Invitrogen), to reduce signal from contaminating DNA, in addition to 10 units of RNaseOUT (Invitrogen) in nuclease free water to make a total of 9µl. The reaction was run in a G-storm Thermal Cycler, for 15 minutes at 37°C and then 15 minutes at 75°C, to deactivate the DNase I enzyme.

For the reverse transcription reaction, the High-Capacity cDNA Reverse Transcription Kit with RNase Inhibitor (Applied Biostystems) was used, following the manufacturer's instructions. In each reaction with RNase inhibitor there was: 0.8µL 100mM dNTP Mix, 2 µL RT Buffer, 2µL 10µm RT Random Primers, 1µL RNase Inhibitor, 1µL Reverse Transcriptase and nuclease-free H2O-up to 20µl. Using the G-storm Thermal Cycler, the reaction was run for 10 minutes at 25°C, which allows primers to bind to the RNA template, 120 minutes at 37°C, to allow cDNA synthesis and 5 minutes at 85°C to deactivate the enzyme. Simultaneously, a negative control which lacked reverse transcriptase, which was substituted for nuclease-free water, was run in the same way, to check for contamination of genomic DNA. cDNA produced from this was then frozen to -20°C, until use.

Quantitative reverse transcription polymerase chain reaction (qRT-PCR)

Many of the primers used had been used previously in qRT-PCR in the Edwards lab, including for the housekeeping gene, *Rps28*, and thus were not tested in this project (sequences presented in the Key Resources Table;(Matarin et al., 2015)). I designed and tested primers for *Mrc1* and *Plcg2*. To allow differentiation between DNA products originating from genomic DNA amplification and cDNA amplification, primers were designed to span different exons in these two genes. Primers were designed using Primer-BLAST (NCBI) which also assesses

their sequence specificity against the entire mouse transcriptome. Once the most specific design had been selected, primers were ordered from Eurofins MWG Operon.

Primers were then tested for specificity for qRT-PCR. In each reaction, 0.25µL of forward and reverse primers (for one gene) were incubated with previously generated cDNA from *App*$^{NL\text{-}G\text{-}F/NL\text{-}G\text{-}F}$ mouse cortex, 10µL of PCR Mix (Bio-Rad) and 7.5µL of nuclease free water. This was then run in the G-storm thermocycler for 3 minutes at 95, then 40 repeats of [95.0°C - 10s, 58.0°C - 30s, 72.0°C -30s], and finally 5 minutes at 72°C to finish. Samples were then run on a 3% agarose gel with ethidium bromide. The results were visualised with the BioRad ChemiDoc MP imaging system. Primers with a single band at the predicted product size with high intensity were selected for further testing. In the no-RT negative controls, bands were not observed.

The next stage of testing for specificity involved linear dilution of the cDNA (starting with neat cDNA and performing serial dilutions by a factor of three up to 1/729) to generate a standard curve. The slope of the standard curve allowed calculation of efficiency of primers and only those with an efficiency of 90-105% were selected for use. In addition, a melt curve analysis was performed to further examine primer specificity by identifying single peaks for the PCR products. These tests ensured the primers would carry out selective and efficient amplification of the desired PCR product, and the linear range of the assay.

qRT-PCR reactions were carried out for all primers, to quantify the levels of specific gene products in cDNA made from RNA isolated from WT and *App*$^{NL\text{-}G\text{-}F/NL\text{-}G\text{-}F}$ mice. SYBR Green PCR mix (Bio-Rad), was mixed with forward and reverse primers (20µm diluted into 180 µm nuclease free water) and cDNA templates. The polymerase chain reaction was run in the CFX96 touch qRT-PCR detection system (Bio-Rad), and the cycling conditions were 3 minutes at 95.0°C, 40 repeats of [95.0°C - 10s, 58.0°C - 30s, 72.0°C -30s] and 5 minutes at 72°C.

In a 96 well plate, each RT sample was tested in triplicate and with one no-RT control. To assess the technical quality of the data, the raw CT values were assessed within triplicates, (i.e. to assess pipetting errors) and the melt curve was analysed for a single PCR product. The CT values for each gene expression in each well were normalised to levels of *Rps28* according to equation: $2^{-(GeneCt-\ Rsp28Ct)}$ (Matarin et al., 2015).

STATISTICAL ANALYSIS

All statistical tests were performed on Prism v6.2 (Graph Pad) or SPSS Statistics 25 (IBM). All results were plotted on Prism v6.2. Data are shown as Mean±SEM and sample size (n) refers to the number of animals in each group. Power analyses were performed for each of the experiments to determine the sample size required (how many animals in each group).

The mean and standard deviation were based on pilot data I had collected in a subset of the exact mice I would use. Mean and standard deviations were used to calculate the Cohen's d value. This was then used to identify the required sample size at a statistical power of 0.8 for the t-test (two-tailed test alpha = 0.05). For immunohistochemistry, at least n=4 mice are needed per group, to detect a >30% difference in cell counts as significant. For example, in the mean IBA1+ cell density between *App*-KI mice and WTs, assuming 16.25±2.22 IBA1+ cells per 100,000µm2, from my pilot microglial counts. For qRT-PCR gene expression n=7 mice were needed per group, to detect >55% difference in gene expression as significant. For example, in the mean *Cd68* expression between *App*-KI mice and WT, assuming 0.14±0.05 expression of *Aif1*, normalised to expression of Rps28 (housekeeping gene), from my preliminary qPCR data.

For RT-qPCR the difference between group means (WT vs $App^{NL\text{-}G\text{-}F/NL\text{-}G\text{-}F}$) for 11 candidate genes tested were analysed with a repeated measures two-way ANOVA with the candidate genes tested and mouse genotype as factors. All 11 genes normalised to *Aif1* expression were analysed together in an ANOVA, except for Aif1 itself, which was analysed with an unpaired two-tailed Students *t*-test between $App^{NL\text{-}G\text{-}F/NL\text{-}G\text{-}F}$ and WT mice and was found not to be significantly different. A Sidak post-hoc test was used to assess significance between genotypes because the two-way ANOVA revealed a significant interaction between candidate gene and mouse genotype. PCR was not performed blind as the analysis was performed by the CFX96 system computer software (BioRad), removing any bias which could influence the results. A custom generalised linear mixed model was used to assess significance of genotype and age within hippocampal region, for immunohistochemistry cell counts, in different regions of CA1 hippocampus in *App*-KI vs WT mice. A Sequential Sidak post-hoc test was used to assess pairwise significance between groups. To reduce experimental bias by preventing any influence on cell counts between genotypes, the cell counting phase of IHC analysis was performed blind. In all cases, if †/*p<0.05 differences were considered significant, alongside ††/**p<0.01, †††/***p<0.001, ††††/****p<0.0001 († corresponds to differences between ages and * corresponds to differences between genotypes).

REFERENCES

Anand, K.S., and Dhikav, V. (2012). Hippocampus in health and disease: An overview. Ann Indian Acad Neurol 15, 239-246.

Braak, H., Alafuzoff, I., Arzberger, T., Kretzschmar, H., and Del Tredici, K. (2006). Staging of Alzheimer disease-associated neurofibrillary pathology using paraffin sections and immunocytochemistry. Acta neuropathologica 112, 389-404.

Brutkiewicz, R.R. (2016). Cell Signaling Pathways That Regulate Antigen Presentation. The Journal of Immunology 197, 2971-2979.

Castillo, E., Leon, J., Mazzei, G., Abolhassani, N., Haruyama, N., Saito, T., Saido, T., Hokama, M., Iwaki, T., Ohara, T.*, et al.* (2017). Comparative profiling of cortical gene expression in Alzheimer's disease patients and mouse models demonstrates a link between amyloidosis and neuroinflammation. Sci Rep 7, 17762.

Cherry, J.D., Olschowka, J.A., and O'Banion, M.K. (2014). Neuroinflammation and M2 microglia: the good, the bad, and the inflamed. J Neuroinflammation 11, 98.

Citron, M., Oltersdorf, T., Haass, C., McConlogue, L., Hung, A.Y., Seubert, P., Vigo-Pelfrey, C., Lieberburg, I., and Selkoe, D.J. (1992). Mutation of the beta-amyloid precursor protein in familial Alzheimer's disease increases beta-protein production. Nature 360, 672-674.

Dagher, N.N., Najafi, A.R., Kayala, K.M., Elmore, M.R., White, T.E., Medeiros, R., West, B.L., and Green, K.N. (2015). Colony-stimulating factor 1 receptor inhibition prevents microglial plaque association and improves cognition in 3xTg-AD mice. J Neuroinflammation 12, 139.

Davalos, D., Grutzendler, J., Yang, G., Kim, J.V., Zuo, Y., Jung, S., Littman, D.R., Dustin, M.L., and Gan, W.B. (2005). ATP mediates rapid microglial response to local brain injury in vivo. Nat Neurosci 8, 752-758.

Elmore, M.R., Najafi, A.R., Koike, M.A., Dagher, N.N., Spangenberg, E.E., Rice, R.A., Kitazawa, M., Matusow, B., Nguyen, H., West, B.L., and Green, K.N. (2014). Colony-stimulating factor 1 receptor signaling is necessary for microglia viability, unmasking a microglia progenitor cell in the adult brain. Neuron 82, 380-397.

Esparza, T.J., Wildburger, N.C., Jiang, H., Gangolli, M., Cairns, N.J., Bateman, R.J., and Brody, D.L. (2016). Soluble Amyloid-beta Aggregates from Human Alzheimer's Disease Brains. Sci Rep 6, 38187.

Esparza, T.J., Zhao, H., Cirrito, J.R., Cairns, N.J., Bateman, R.J., Holtzman, D.M., and Brody, D.L. (2013). Amyloid-beta oligomerization in Alzheimer dementia versus high-pathology controls. Ann Neurol 73, 104-119.

Fan, Z., Brooks, D.J., Okello, A., and Edison, P. (2017). An early and late peak in microglial activation in Alzheimer's disease trajectory. Brain : a journal of neurology 140, 792-803.

Fonseca, M.I., Chu, S.H., Hernandez, M.X., Fang, M.J., Modarresi, L., Selvan, P., MacGregor, G.R., and Tenner, A.J. (2017). Cell-specific deletion of C1qa identifies microglia as the dominant source of C1q in mouse brain. J Neuroinflammation 14, 48.

Guardia-Laguarta, C., Pera, M., Clarimon, J., Molinuevo, J.L., Sanchez-Valle, R., Llado, A., Coma, M., Gomez-Isla, T., Blesa, R., Ferrer, I., and Lleo, A. (2010). Clinical, neuropathologic, and biochemical profile of the amyloid precursor protein I716F mutation. J Neuropathol Exp Neurol 69, 53-59.

Guerreiro, R., Wojtas, A., Bras, J., Carrasquillo, M., Rogaeva, E., Majounie, E., Cruchaga, C., Sassi, C., Kauwe, J.S., Younkin, S.*, et al.* (2013). TREM2 variants in Alzheimer's disease. N Engl J Med 368, 117-127.

Haass, C., Kaether, C., Thinakaran, G., and Sisodia, S. (2012). Trafficking and proteolytic processing of APP. Cold Spring Harbor perspectives in medicine 2, a006270.

Hamelin, L., Lagarde, J., Dorothee, G., Leroy, C., Labit, M., Comley, R.A., de Souza, L.C., Corne, H., Dauphinot, L., Bertoux, M.*, et al.* (2016). Early and protective microglial activation in Alzheimer's disease: a prospective study using 18F-DPA-714 PET imaging. Brain : a journal of neurology 139, 1252-1264.

Hanisch, U.K., and Kettenmann, H. (2007). Microglia: active sensor and versatile effector cells in the normal and pathologic brain. Nat Neurosci 10, 1387-1394.

Hong, S., Beja-Glasser, V.F., Nfonoyim, B.M., Frouin, A., Li, S., Ramakrishnan, S., Merry, K.M., Shi, Q., Rosenthal, A., Barres, B.A.*, et al.* (2016). Complement and microglia mediate early synapse loss in Alzheimer mouse models. Science 352, 712-716.

Hoozemans, J.J.M., Veerhuis, R., Rozemuller, J.M., and Eikelenboom, P. (2006). Neuroinflammation and regeneration in the early stages of Alzheimer's disease pathology. International Journal of Developmental Neuroscience 24, 157-165.
Hopperton, K.E., Mohammad, D.T., M.O. , Giuliano, V., and Bazinet, R.P. (2018). Markers of microglia in post-mortem brain samples from patients with Alzheimer's disease: a systematic review. Mol Psychiatry 23, 177–198.
Imai, Y., Ibata, I., Ito, D., Ohsawa, K., and Kohsaka, S. (1996). A novel gene iba1 in the major histocompatibility complex class III region encoding an EF hand protein expressed in a monocytic lineage. Biochem Biophys Res Commun 224, 855-862.
Itagaki, S., McGeer, P.L., Akiyama, H., Zhu, S., and Selkoe, D. (1989). Relationship of microglia and astrocytes to amyloid deposits of Alzheimer disease. J Neuroimmunol 24, 173-182.
Ito, D., Imai, Y., Ohsawa, K., Nakajima, K., Fukuuchi, Y., and Kohsaka, S. (1998). Microglia-specific localisation of a novel calcium binding protein, Iba1. Brain Res Mol Brain Res 57, 1-9.
Jimenez, S., Baglietto-Vargas, D., Caballero, C., Moreno-Gonzalez, I., Torres, M., Sanchez-Varo, R., Ruano, D., Vizuete, M., Gutierrez, A., and Vitorica, J. (2008). Inflammatory response in the hippocampus of PS1M146L/APP751SL mouse model of Alzheimer's disease: age-dependent switch in the microglial phenotype from alternative to classic. J Neurosci 28, 11650-11661.
Jonsson, T., Stefansson, H., Steinberg, S., Jonsdottir, I., Jonsson, P.V., Snaedal, J., Bjornsson, S., Huttenlocher, J., Levey, A.I., Lah, J.J.*, et al.* (2013). Variant of TREM2 associated with the risk of Alzheimer's disease. N Engl J Med 368, 107-116.
Kleinberger, G., Yamanishi, Y., Suarez-Calvet, M., Czirr, E., Lohmann, E., Cuyvers, E., Struyfs, H., Pettkus, N., Wenninger-Weinzierl, A., Mazaheri, F.*, et al.* (2014). TREM2 mutations implicated in neurodegeneration impair cell surface transport and phagocytosis. Sci Transl Med 6, 243ra286.
Koenigsknecht-Talboo, J., and Landreth, G.E. (2005). Microglial phagocytosis induced by fibrillar beta-amyloid and IgGs are differentially regulated by proinflammatory cytokines. J Neurosci 25, 8240-8249.
Krasemann, S., Madore, C., Cialic, R., Baufeld, C., Calcagno, N., El Fatimy, R., Beckers, L., O'Loughlin, E., Xu, Y., Fanek, Z.*, et al.* (2017). The TREM2-APOE Pathway Drives the Transcriptional Phenotype of Dysfunctional Microglia in Neurodegenerative Diseases. Immunity 47, 566-581 e569.
Kuno, R., Wang, J., Kawanokuchi, J., Takeuchi, H., Mizuno, T., and Suzumura, A. (2005). Autocrine activation of microglia by tumor necrosis factor-alpha. J Neuroimmunol 162, 89-96.
Lambert, J.C., Ibrahim-Verbaas, C.A., Harold, D., Naj, A.C., Sims, R., Bellenguez, C., DeStafano, A.L., Bis, J.C., Beecham, G.W., Grenier-Boley, B.*, et al.* (2013). Meta-analysis of 74,046 individuals identifies 11 new susceptibility loci for Alzheimer's disease. Nat Genet 45, 1452-1458.
Liu, W. (2017). The cellular functions of TREM2 in microglia in relation to Alzheimer's disease. Doctoral thesis (PhD), UCL (University College London).
Maezawa, I., Zimin, P.I., Wulff, H., and Jin, L.W. (2011). Amyloid-beta protein oligomer at low nanomolar concentrations activates microglia and induces microglial neurotoxicity. The Journal of biological chemistry 286, 3693-3706.
Martin, E., Boucher, C., Fontaine, B., and Delarasse, C. (2017). Distinct inflammatory phenotypes of microglia and monocyte-derived macrophages in Alzheimer's disease models: effects of aging and amyloid pathology. Aging Cell 16, 27-38.
Matarin, M., Salih, D.A., Yasvoina, M., Cummings, D.M., Guelfi, S., Liu, W., Nahaboo Solim, M.A., Moens, T.G., Paublete, R.M., Ali, S.S.*, et al.* (2015). A genome-wide gene-expression analysis and database in transgenic mice during development of amyloid or tau pathology. Cell Rep 10, 633-644.
Matsumura, A., Suzuki, S., Iwahara, N., Hisahara S, Kawamata J, Suzuki H, Yamauchi A, T.K., Kitamura Y, and S, S. (2015). Temporal changes of CD68 and α7 nicotinic acetylcholine receptor expression in microglia in Alzheimer's disease-like mouse models. Journal of ALzheimer's Disease 44, 409-423.
McGeer, P.L., Itagaki, S., Tago, H., and McGeer, E.G. (1987). Reactive microglia in patients with senile dementia of the Alzheimer type are positive for the histocompatibility glycoprotein HLA-DR. Neurosci Lett 79, 195-200.
Michelucci, A., Heurtaux, T., Grandbarbe, L., Morga, E., and Heuschling, P. (2009). Characterization of the microglial phenotype under specific pro-inflammatory and anti-

inflammatory conditions: Effects of oligomeric and fibrillar amyloid-beta. J Neuroimmunol 210, 3-12.
Minett, T., Classey, J., Matthews, F.E., Fahrenhold, M., Taga, M., Brayne, C., Ince, P.G., Nicoll, J.A., Boche, D., and Mrc, C. (2016). Microglial immunophenotype in dementia with Alzheimer's pathology. J Neuroinflammation 13, 135.
Morganti, J.M., Riparip, L.K., and Rosi, S. (2016). Call Off the Dog(ma): M1/M2 Polarization Is Concurrent following Traumatic Brain Injury. PLoS One 11, e0148001.
Mosser, D.M., and Edwards, J.P. (2008). Exploring the full spectrum of macrophage activation. Nat Rev Immunol 8, 958-969.
Nimmerjahn, A., Kirchhoff, F., and Helmchen, F. (2005). Resting microglial cells are highly dynamic surveillants of brain parenchyma in vivo. Science 308, 1314-1318.
Ohsawa, K., Imai, Y., Sasaki, Y., and Kohsaka, S. (2004). Microglia/macrophage-specific protein Iba1 binds to fimbrin and enhances its actin-bundling activity. J Neurochem 88, 844-856.
Olah, M., Patrick, E., Villani, A.C., Xu, J., White, C.C., Ryan, K.J., Piehowski, P., Kapasi, A., Nejad, P., Cimpean, M.*, et al.* (2018). A transcriptomic atlas of aged human microglia. Nat Commun 9, 539.
Olmos-Alonso, A., Schetters, S.T., Sri, S., Askew, K., Mancuso, R., Vargas-Caballero, M., Holscher, C., Perry, V.H., and Gomez-Nicola, D. (2016). Pharmacological targeting of CSF1R inhibits microglial proliferation and prevents the progression of Alzheimer's-like pathology. Brain : a journal of neurology.
Perlmutter, L.S., Scott, S.A., Barron, E., and Chui, H.C. (1992). MHC class II-positive microglia in human brain: association with Alzheimer lesions. J Neurosci Res 33, 549-558.
Revett, T.J., Baker, G.B., Jhamandas, J., and Kar, S. (2013). Glutamate system, amyloid ss peptides and tau protein: functional interrelationships and relevance to Alzheimer disease pathology. J Psychiatry Neurosci 38, 6-23.
Saito, T., Matsuba, Y., Mihira, N., Takano, J., Nilsson, P., Itohara, S., Iwata, N., and Saido, T.C. (2014). Single App knock-in mouse models of Alzheimer's disease. Nat Neurosci 17, 661-663.
Shankar, G.M., Li, S., Mehta, T.H., Garcia-Munoz, A., Shepardson, N.E., Smith, I., Brett, F.M., Farrell, M.A., Rowan, M.J., Lemere, C.A.*, et al.* (2008). Amyloid-beta protein dimers isolated directly from Alzheimer's brains impair synaptic plasticity and memory. Nat Med 14, 837-842.
Sims, R., van der Lee, S.J., Naj, A.C., Bellenguez, C., Badarinarayan, N., Jakobsdottir, J., Kunkle, B.W., Boland, A., Raybould, R., Bis, J.C.*, et al.* (2017). Rare coding variants in PLCG2, ABI3, and TREM2 implicate microglial-mediated innate immunity in Alzheimer's disease. Nat Genet 49, 1373-1384.
Smith, A.M., Gibbons, H.M., Oldfield, R.L., Bergin, P.M., Mee, E.W., Faull, R.L., and Dragunow, M. (2013). The transcription factor PU.1 is critical for viability and function of human brain microglia. Glia 61, 929-942.
Suarez-Calvet, M., Kleinberger, G., Araque Caballero, M.A., Brendel, M., Rominger, A., Alcolea, D., Fortea, J., Lleo, A., Blesa, R., Gispert, J.D.*, et al.* (2016). sTREM2 cerebrospinal fluid levels are a potential biomarker for microglia activity in early-stage Alzheimer's disease and associate with neuronal injury markers. EMBO Mol Med 8, 466-476.
Thal, D.R., Rub, U., Orantes, M., and Braak, H. (2002). Phases of A beta-deposition in the human brain and its relevance for the development of AD. Neurology 58, 1791-1800.
Tsubuki, S., Takaki, Y., and Saido, T.C. (2003). Dutch, Flemish, Italian, and Arctic mutations of APP and resistance of Abeta to physiologically relevant proteolytic degradation. Lancet 361, 1957-1958.
Walker, D.G., and Lue, L.F. (2015). Immune phenotypes of microglia in human neurodegenerative disease: challenges to detecting microglial polarization in human brains. Alzheimers Res Ther 7, 56.
Walton, M.R., Gibbons, H., MacGibbon, G.A., Sirimanne, E., Saura, J., Gluckman, P.D., and Dragunow, M. (2000). PU.1 expression in microglia. J Neuroimmunol 104, 109-115.
Wang, W.Y., Tan, M.S., Yu, J.T., and Tan, L. (2015). Role of pro-inflammatory cytokines released from microglia in Alzheimer's disease. Ann Transl Med 3, 136.
Yamada, K., Yabuki, C., Seubert, P., Schenk, D., Hori, Y., Ohtsuki, S., Terasaki, T., Hashimoto, T., and Iwatsubo, T. (2009). Abeta immunotherapy: intracerebral sequestration of Abeta by an anti-Abeta monoclonal antibody 266 with high affinity to soluble Abeta. J Neurosci 29, 11393-11398.

Yin, Z., Raja, D., Saiepour, N., Van Dam, D., Brouwer, N., Holtman, I.R., Eggena, B., Möller, T., Tamm, J.A., Abdourahman, A.*, et al.* (2017). Immune hyperreactivity of Aβ plaque-associated microglia in Alzheimer's disease. Neurobiol Aging 55, 115-122.
Zhao, Y., Wu, X., Li, X., Jiang, L.L., Gui, X., Liu, Y., Sun, Y., Zhu, B., Pina-Crespo, J.C., Zhang, M.*, et al.* (2018). TREM2 Is a Receptor for beta-Amyloid that Mediates Microglial Function. Neuron 97, 1023-1031 e1027.